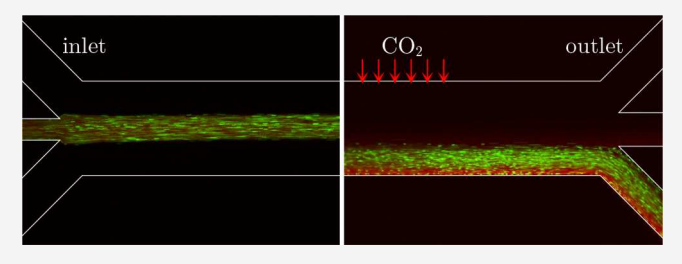
Downloaded via OKINAWA INST SCI TECHLGY GRAD UNIV on January 14, 2020 at 13:07:29 (UTC). See https://pubs.acs.org/sharingguidelines for options on how to legitimately share published articles.

Colloid Separation by CO₂-Induced Diffusiophoresis

Trevor J. Shimokusu,[†] Vanessa G. Maybruck,[‡] Jesse T. Ault,[¶] and Sangwoo Shin*,[†]

ABSTRACT: We present a microfluidic crossflow separation of colloids enabled by the dissolution of CO₂ gas in aqueous suspensions. The dissolved CO₂ dissociates into H⁺ and HCO₃⁻ ions, which are efficient candidates for electrolytic diffusiophoresis, because of the fast diffusion of protons. By exposing CO₂ gas to one side of a microfluidic flow channel, a crossflow gradient can be created, enabling the crossflow diffusiophoresis of suspended particles. We develop a simple two-dimensional model to describe the coupled transport



dynamics that is due to the competition of advection and diffusiophoresis. Furthermore, we show that oil nanoemulsions can be effectively separated by utilizing highly charged particles as a carrier vehicle, which is otherwise difficult to achieve. These results demonstrate a portable, versatile method for separating particles in broad applications including oil extraction, drug delivery, and bioseparation.

INTRODUCTION

Manipulating the motion of colloidal particles in a controllable manner is critical for the development and enhancement of separation processes. With the advent of microfluidics and soft lithography, the field of separations has grown enormously over the last few decades. Simple fabrication processes enabled by soft lithography and other technologies have enabled detailed studies on various migration mechanisms that can be utilized for controlling the motion of particles such as electrophoresis, dielectrophoresis, acoustophoresis, thermophoresis, a inertial migration, optophoresis, magnetophoresis,⁷ and diffusiophoresis.⁸

Among these methods, there has been a growing interest in diffusiophoresis over the recent years (apart from active matter) $^{9-40}$ (recent review articles include refs 41–43). Diffusiophoresis describes the motion of colloidal particles induced by nonequilibrium interactions (which are usually attractive) between the particles and the surrounding solute molecules.⁴⁴ When such a particle is exposed to a solute concentration gradient, an osmotic pressure imbalance within the interaction region induces a fluid flow, resulting in particle migration in the direction opposite to this interfacial fluid flow, through a process known as chemiphoresis. In addition, when the solutes are ionic, a local diffusion potential develops, because of the diffusivity contrast between the solute species. This local potential, in turn, can induce the electrophoresis of a charged particle. The particle diffusiophoretic velocity is expressed as $\mathbf{u}_{dp} = \Gamma \nabla \ln c$, where *c* is the solute concentration, and Γ is the particle diffusiophoretic mobility, which is a transport coefficient that describes the efficacy of particle diffusiophoresis for a given particle-solute pair. The diffusiophoretic mobility can also be expressed as $\Gamma = \Gamma_{cp}$ + $\Gamma_{\rm ep}$, where $\Gamma_{\rm cp}$ and $\Gamma_{\rm ep}$ denote, respectively, the contributions

due to chemiphoresis and electrophoresis. For a charged particle immersed in a symmetric electrolyte, the diffusiophoretic mobility Γ is sensitive to the particle zeta potential ζ and the normalized solute diffusivity contrast, $\beta = (D_+ - D_-)/(D_+$ + D_{-}), where D_{+} and D_{-} are, respectively, the diffusivity of the cation and the anion.

The key advantage of diffusiophoresis for separation purposes is the ability to separate without the need of any external power sources or other bulky peripheral components, thus facilitating portable, low-cost, and simple separation techniques. This advantage has motivated many studies of the crossflow separation of various colloidal particles, including polystyrene latex,⁸ E. coli,⁴⁵ urease enzymes,⁴⁶ and TiO₂ nanoparticles.⁴⁷ However, one potential disadvantage of the use of diffusiophoresis in separations is that the addition of solute to the particle stream may be undesirable for certain applications that are solute-sensitive or require post-separation removal of the solute.

Recently, we have demonstrated the use of CO2 gas to drive particle diffusiophoresis.²¹ Because of the ability of CO₂ gas to naturally equilibrate with an aqueous solution, any dissolved CO₂ and corresponding ionic species can be easily removed from solution by equilibrating back to the atmospheric conditions. In this regard, the use of CO₂ is attractive for diffusiophoretic separations, since removal of the solute is simple and efficient. Furthermore, we have shown that the use of polydimethylsiloxane (PDMS) as a gas permeable

Special Issue: Advances in Active Materials

Received: October 30, 2019 Revised: December 17, 2019 Published: December 20, 2019

Department of Mechanical Engineering, University of Hawaii at Manoa, Honolulu, Hawaii 96822, United States

^{*}Computational Sciences and Engineering Division, Oak Ridge National Laboratory, Oak Ridge, Tennessee 37831, United States [¶]School of Engineering, Brown University, Providence, Rhode Island 02912, United States

membrane can allow a continuous, efficient, and scalable particle separation method via diffusiophoresis that does not require any additional mixing stream.²¹

In this paper, we investigate the microfluidic crossflow separation of colloids enabled by CO₂-driven diffusiophoresis. We use experiments and theoretical analysis to (i) gain a deeper understanding of the coupled transport phenomena that are involved and (ii) provide engineering design guidelines for such a separation process. Finally, we demonstrate a novel approach for the separation of nanoemulsions through the use of charged carrier vehicle particles, which is otherwise difficult to achieve.

MATERIALS AND METHODS

Materials. Carboxylate-functionalized polystyrene latex particles (diameter = 1 μ m) were purchased from ThermoFisher Scientific. Amine-functionalized polystyrene latex particles (diameter = 1 μ m) were purchased from Sigma-Aldrich. Polystyrene nanoparticles (diameter = 50 nm) were purchased from Bangs Laboratory. Decane and 3-aminopropyltrimethoxysilane (APTES) were purchased from Sigma-Aldrich. PDMS was purchased from Dow Corning. Oilsoluble fluorescent dye was purchased from Tracer Products.

Microfluidics Experiments. Microfluidic devices were fabricated from PDMS using a conventional soft lithography technique. 48 Since the gas permeability of PDMS is known to be dependent on the monomer/cross-linker mixing ratio and the curing temperature, 49 we chose a mixing ratio of 10:1 and a curing temperature of 75°C. The inlet streams were injected into the microfluidic channel by a syringe pump (Pump 11 Pico Plus Elite, Harvard Apparatus). To prevent adhesion of amine-functionalized polystyrene particles on to the PDMS channel surface, a 1 vol % aqueous solution of 3-aminopropyltrimethoxysilane was flowed through the channel for 30 min, followed by a rinsing cycle with deionized water for 10 min. 50 The colloidal particles and oil emulsion were suspended in deionized water (Direct Q3, Millipore). Decane nanoemulsions were produced by sonicating decane for 5 min (Fisher Scientific) followed by vortex mixing for 10 s (VWR). The particle zeta potential was measured by electrophoretic light scattering (Zetasizer Nano-ZS, Malvern Panalytical). The particles were visualized with an inverted fluorescence microscope (DMi8, Leica) and analyzed using ImageJ.

■ RESULTS AND DISCUSSION

Crossflow Particle Migration by CO₂ Dissolution. The experimental setup is presented in Figure 1. The main flow channel of the microfluidic device used is 30 mm in length (L), 200 μ m in width (w), and 20 μ m in height (h). Flow through this channel is fed from a centered inlet channel (40 μ m wide) carrying the particle suspension and two sheath flow inlet channels, which are each 80 μ m wide. At the other end of the main flow channel, the flow exits through three outlets of equal width.

In the microfluidic device, CO_2 gas at an elevated pressure of 186 kPa was fed through a channel adjacent to the main flow channel, while another identical channel located on the opposite side of the main channel was open to the atmosphere (Figure 1b). This design allows CO_2 to permeate through the thin PDMS wall (thickness $\approx 35~\mu m$), which subsequently dissolves into the main particle stream, thereby introducing the crossflow CO_2 concentration gradient needed to drive diffusiophoresis. The air channel facilitates the degassing of the dissolved CO_2 and effectively serves as a sink for maintaining a constant transverse gradient throughout the channel.

When CO₂ gas dissolves in water, the dissolved gas molecules form an equilibrium with H⁺ and HCO₃⁻ ions.

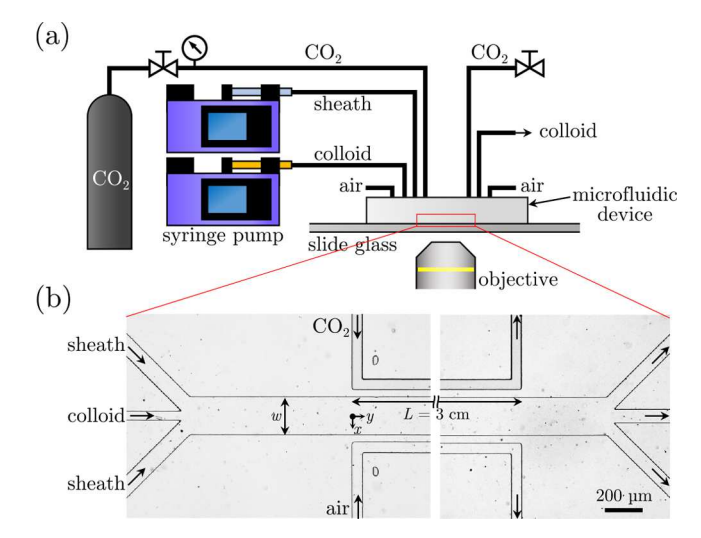


Figure 1. Experimental setup. (a) Schematic of the complete experimental setup. The microfluidic device consists of a main flow channel comprised of two sheath flow inlets, a centered flow inlet carrying the particle solution, three outlets of equal widths, a CO_2 gas channel connected to a CO_2 gas supply and pressure regulator, and an air channel open to atmosphere. (b) Bright-field microscope image of the channel.

The constituent ions H⁺ and HCO₃⁻ yield a large normalized solute diffusivity contrast of $\beta = 0.77$, because of the fast diffusivity of protons (cf. for most inorganic salts, $-0.4 < \beta < 0.4$ (ref 41)). Such a large β suggests that this ion combination has the potential to induce strong electrolytic diffusiophoresis.

As the colloidal particles are advected downstream along the flow channel, the ion concentration gradient drives particle migration in the transverse direction. As shown in Figure 2a,

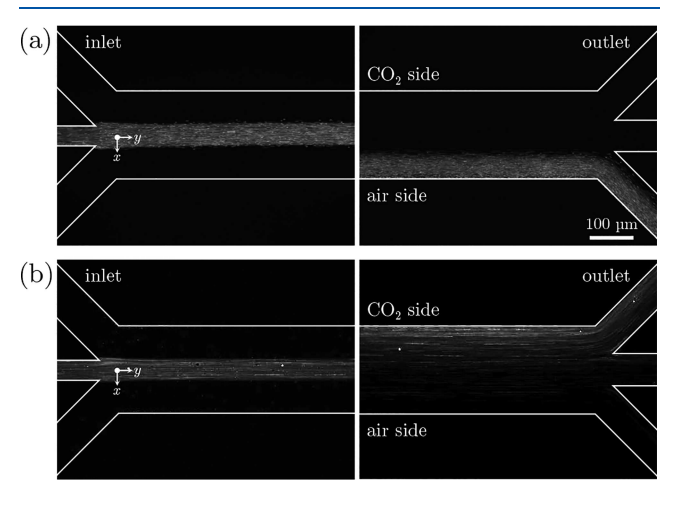


Figure 2. Lateral migration of colloidal particles via ${\rm CO_2}$ -induced diffusiophoresis. Fluorescence microscope images of (a) carboxylate-functionalized polystyrene (cPS) particles and (b) amine-functionalized polystyrene (aPS) particles near the inlet and the outlet regions. The mean flow speed in the main flow channel is $\overline{U}=0.35$ mm/s.

the transverse position of a stream of negatively charged particles (carboxylate-modified polystyrene (cPS), zeta potential $\zeta=-75$ mV) is observed to shift away from the CO₂ source at locations downstream (positive *x*-direction). While chemiphoresis always acts to drive particles in the direction of increasing solute concentration, the direction of electrophoresis is dependent on the signs of the particle zeta

potential and the β value. In the case of the H⁺/HCO₃⁻ ion pair diffusing away from the CO₂ boundary, the electric field is set in the negative x-direction. Thus, negatively charged particles experience electrophoresis directed in the positive x-direction. This suggests that, for this particle/solute combination, the electrophoresis and chemiphoresis are competing processes; however, because of the large β value, electrophoresis dominates, and the resulting particle motion is in the positive x-direction.

In contrast, with the same solute concentration gradient, and, thus, the same electric field, a stream of positively charged particles (amine-modified polystyrene (aPS), $\zeta = +60$ mV) is observed to migrate in the opposite direction, deflecting toward the CO₂ side (Figure 2b). In this case, electrophoresis and chemiphoresis act in concert, resulting in an upward deflection (i.e., negative α -direction) of the aPS particle stream, in contrast to the downward deflection displayed by the cPS particles.

In addition to migrating in opposite directions, the manner in which the oppositely charged particles are deflected also differs noticeably. This difference in migration behaviors is shown in Figures 3a and 3d. While the cPS particles have a

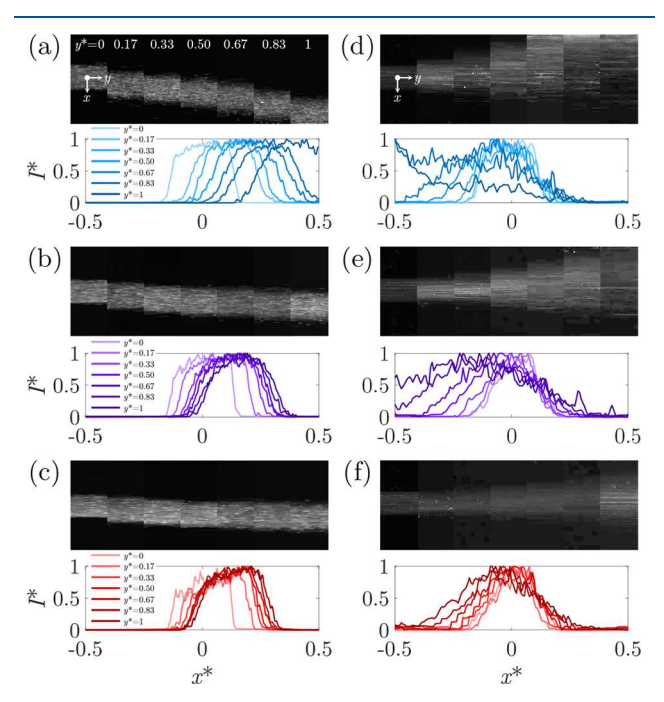


Figure 3. Transverse particle migration of (a–c) cPS and (d–f) aPS particles by diffusiophoresis. The top panels show snapshots of fluorescence images at downstream locations $y^* = y/L$. The bottom panel shows the normalized intensity distribution $I^* = I/I_{\text{max}}$ where I_{max} is the maximum pixel intensity in the transverse direction $x^* = x/w$. Panels (a) and (d), $\overline{U} = 0.35 \text{ mm/s}$ [(a) Pe* = 0.17, (d) Pe* = 0.11]; panels (b) and (e), $\overline{U} = 0.69 \text{ mm/s}$ [(b) Pe* = 0.34, (e) Pe* = 0.23]; and panels (c) and (f), $\overline{U} = 1.04 \text{ mm/s}$ [(c) Pe* = 0.51, (f) Pe* = 0.34].

tendency to migrate gradually altogether without experiencing significant dispersion, the aPS particle stream disperses during deflection, subsequently leading to particle accumulation near the wall. This behavior originates from the nonlinear nature of diffusiophoresis in which the particle migration is sensitive to the gradient of the logarithm of the solute concentration. ^{28,51} These behaviors are related to previously observed particle dynamics in which particles traveling up a solute gradient by

diffusiophoresis have a tendency to focus into bands, whereas particles traveling down gradients have a tendency to diffuse as they migrate. ^{24,52} These behaviors result in a diffuse, gradually decaying distribution of aPS particles and a relatively flat, constant distribution of cPS particles.

For a given particle mobility, the transverse particle location at a fixed position downstream, which is directly related to the separation efficacy, is dependent on the balance between advection and diffusiophoretic migration. Intuitively, a simple approach to quantifying the separation efficiency is to compare the transverse diffusiophoretic migration time scale $t_{\rm dp}$ ($t_{\rm dp}\approx w^2/|\Gamma|$) and the advective particle residence time scale $t_{\rm ad}$ ($t_{\rm ad}\approx L/\bar{U}$). These can be combined into a Peclet number (Pe), which highlights the competing effects between the diffusiophoresis and advection, which are controlled by the particle type and the flow rate, respectively.

$$Pe^* = \frac{\overline{U}w^2}{|\Gamma|L}$$

Figure 3 demonstrates the streamwise particle distributions and the corresponding transverse fluorescence intensity distributions for various Pe^* . From these data, the mean transverse particle locations can be obtained by calculating $\langle x^* \rangle$:

$$\langle x^* \rangle = \frac{\int x^* I \, \mathrm{d}x^*}{\int I \, \mathrm{d}x^*}$$

where I is the pixel intensity. These results are presented in Figure 4a.

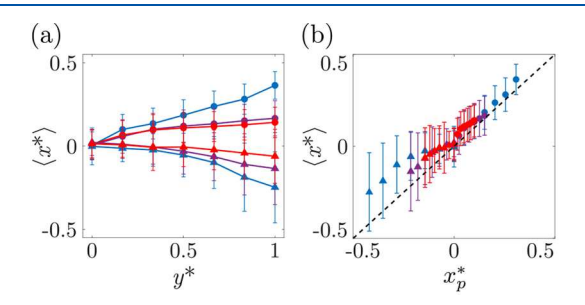


Figure 4. (a) Mean transverse location of the particles, $\langle x^* \rangle$. Circles and triangles represent cPS and aPS particles, respectively. Blue, purple, and red curves represent $\overline{U}=0.35,\ 0.69,\ \text{and}\ 1.04\ \text{mm/s},$ respectively. The error bars represent 2σ , where $\sigma=0.35$

$$\sqrt{\frac{\int (x^* - \langle x^* \rangle)^2 I \, dx^*}{\int I \, dx^*}}$$
. (b) Comparison between the experimental mean

transverse location of the particles and the theoretical prediction for the trajectory of a single nondiffusive particle, xp^* , which is given in eq 2.

Based on a simple balance of the diffusiophoretic and advective time scales, the mean transverse location of the particle stream, $\langle x^* \rangle$, at a fixed y^* could be expected to scale as Pe^{*-1} . For small deviations of the particle stream, this scaling does appear to hold for both aPS and cPS particles. However, this scaling does not account for the nonlinear dependence of diffusiophoretic velocity on the solute concentration. When particles experience larger deflections, they effectively move into regions of higher or lower solute concentration, resulting in a different diffusiophoretic velocity, and a constantly changing diffusiophoretic time scale. Thus, a more rigorous

analysis is needed that accounts for the nonlinear dependence of diffusiophoretic velocity on solute concentration.

We consider the motion of a single suspended particle in a simple two-dimensional approximation of our flow system. Here, we assume that the fluid velocity is simply $\mathbf{u}_{\rm f}=0\mathbf{i}+\overline{U}\mathbf{j}+0\mathbf{k}$. Furthermore, we assume that the ion concentration is only a function of x, and varies linearly between the two walls, where the ion concentration at the walls are fixed at c_1 ($c_1=c(x^*=-0.5)$) and c_2 ($c_2=c(x^*=0.5)$). This is justified by the fact that the transverse solute diffusion time $t_{\rm s}\approx w^2/D_{\rm s}\approx 19~{\rm s}$ is much smaller than the particle residence time $t_{\rm ad}\approx L/\overline{U}$, which varies from 29 s to 86 s, depending on \overline{U} . Here, $D_{\rm s}$ is the ambipolar solute diffusivity ($D_{\rm s}=\frac{2D_{\rm s}D_{\rm s}}{D_{\rm s}+D_{\rm s}}=2.1\times 10^{-9}~{\rm m}^2/{\rm s}$).

Moreover, the transverse diffusion of the solutes is further accelerated by Taylor dispersion as the current transport conditions fall under the Taylor dispersion regime, i.e., $1 \ll Pe$ = $\frac{\bar{U}_W}{2D_c} \ll \frac{2L}{w}$. S In fact, full three-dimensional (3-D) simulations

of the Navier–Stokes equation and the coupled advection diffusion equation for the solute were solved using Open-FOAM of the real physical geometry of the system. These simulations were performed in order to determine the entrance length of the solute concentration profile in the main straight section of the systems. From these results, we determined that the solute concentration profile becomes fully developed before $y^* = 0.1$, which allows us to assume a linear concentration profile throughout the system for the purposes of the model. The velocity of a single particle then is given by $\mathbf{u}_p = \mathbf{u}_f + \mathbf{u}_{dp}$, which becomes

$$\mathbf{u}_{p} = \Gamma \frac{\mathrm{d} \ln c}{\mathrm{d}x} \mathbf{i} + \overline{U} \mathbf{j} + 0 \mathbf{k} \tag{1}$$

This can be directly integrated using an initial particle position of $x_p = y_p = z_p = 0$ to give

$$\frac{x_{p}}{w} = \left(\frac{c_{1} + c_{2}}{c_{1} - c_{2}}\right) \left[1 - \sqrt{1 + \frac{2y_{p}\Gamma}{\bar{U}w^{2}} \left(\frac{c_{1} - c_{2}}{c_{1} + c_{2}}\right)^{2}}\right]$$
(2)

We compare this theoretical prediction for $x_P^* = x_p/w$ with the experimental value of $\langle x^* \rangle$ in Figure 4b. As can be seen, there is reasonable agreement between this simple two-dimensional (2-D) prediction and the experimentally measured values over a range of flow rates for both aPS and cPS particles. Here, we have chosen a value of $(c_1 + c_2)/(c_1 - c_2) = 5$ as a fitting parameter, because of the difficulty in measuring the exact CO₂ and/or ion concentrations experienced at the walls.

Note that this result is applicable to any field flow fractionation system that uses diffusiophoresis as the driving cross-flow mechanism under the assumptions of (1) shallow channel depth (such that the depth-averaged flow velocity is approximately equal to the area-averaged velocity), (2) fixed, uniform solute concentrations at the two walls, and (3) the flow rate is small enough that the diffusive time scale of the solute ions is fast, relative to the advective time scale along the flow (such that the solute profile is approximately linear throughout).

Size Effect. Because the ion concentration in solution is low (O(0.1) mM), the Debye layer thickness κ^{-1} is nonnegligible, compared to the particle radius a. In contrast to the typical treatments of diffusiophoresis or electrophoresis as a size-independent phenomenon under the thin Debye layer limit, 54,55 the current system requires us to consider

diffusiophoresis as a size-dependent mechanism. Keh and Wei previously obtained an analytical solution for size-dependent diffusiophoresis at an arbitrary Debye layer thickness for small zeta potentials. Using a regular perturbation expansion with ζ as the perturbation parameter, the expression for the size-dependent diffusiophoretic mobility $\Gamma(\kappa a)$ in a symmetric electrolyte is given as

$$\Gamma(\kappa a) = \frac{\epsilon}{\eta} \left[\frac{kT}{Ze} \beta \Theta_1(\kappa a) \zeta + \frac{1}{8} \Theta_2(\kappa a) \zeta^2 + O(\zeta^3) \right]$$
(3)

where ϵ is the solution permittivity, η the viscosity, k the Boltzmann constant, T the temperature, Z the valence, and ϵ the elementary charge. The Θ functions are given by

$$\Theta_1(x) = 1 - e^x [5E_7(x) - 2E_5(x)]$$
(4a)

$$\Theta_{2}(x) = 1 + e^{x} \left[4E_{3}(x) + 12E_{4}(x) - \frac{28}{3}E_{5}(x) - 20E_{6}(x) \right]$$

$$+ e^{2x} \left[\frac{10}{3}E_{6}(2x) + \frac{7}{3}E_{8}(2x) - 40E_{3}(x)E_{7}(x) - 40E_{5}(x)E_{7}(x) \right]$$
(4b)

where $E_n(x) = \int_1^\infty t^{-n} e^{-xt} dt$ is the exponential integral of order

Because electrophoresis and chemiphoresis act in the opposite directions for negatively charged particles, the size dependence exhibits a peculiar behavior in which the finite size effect actually *enhances* diffusiophoresis (Figure 5a). It is

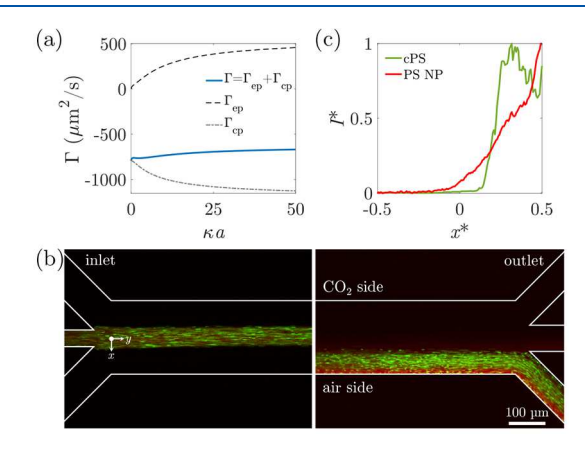


Figure 5. Size-dependent diffusiophoresis. (a) Electrophoretic mobility $\Gamma_{\rm ep}$ (dashed curve) and chemiphoretic mobility $\Gamma_{\rm cp}$ (dash-dotted curve), with respect to κa . The blue curve represents the diffusiophoretic mobility $\Gamma = \Gamma_{\rm cp} + \Gamma_{\rm ep}$. (b) Fluorescence images of a mixture of cPS particles and polystyrene nanoparticles (PS NP) near the inlet and the outlet regions. Green indicates cPS and red indicates PS NP. The mean flow speed is $\bar{U}=0.35$ mm/s. (c) Fluorescence intensity distribution in the crossflow direction for cPS (green) and PS NP (red).

known that the size effect generally suppresses diffusiophoresis, 17,55 which is indeed demonstrated by the electrophoresis and chemiphoresis curves in Figure 5a. However, the competition between electrophoresis and chemiphoresis causes the size effect to work in reverse, such that the overall diffusiophoresis increases as the particle size becomes smaller. For example, in the current system, polystyrene nanoparticles with radii of a=25 nm show a 16% higher diffusiophoretic mobility, compared to the cPS particles with a=500 nm, which have a similar zeta potential. Note that the diffusiophoretic mobility of similar nanoparticles show 40%

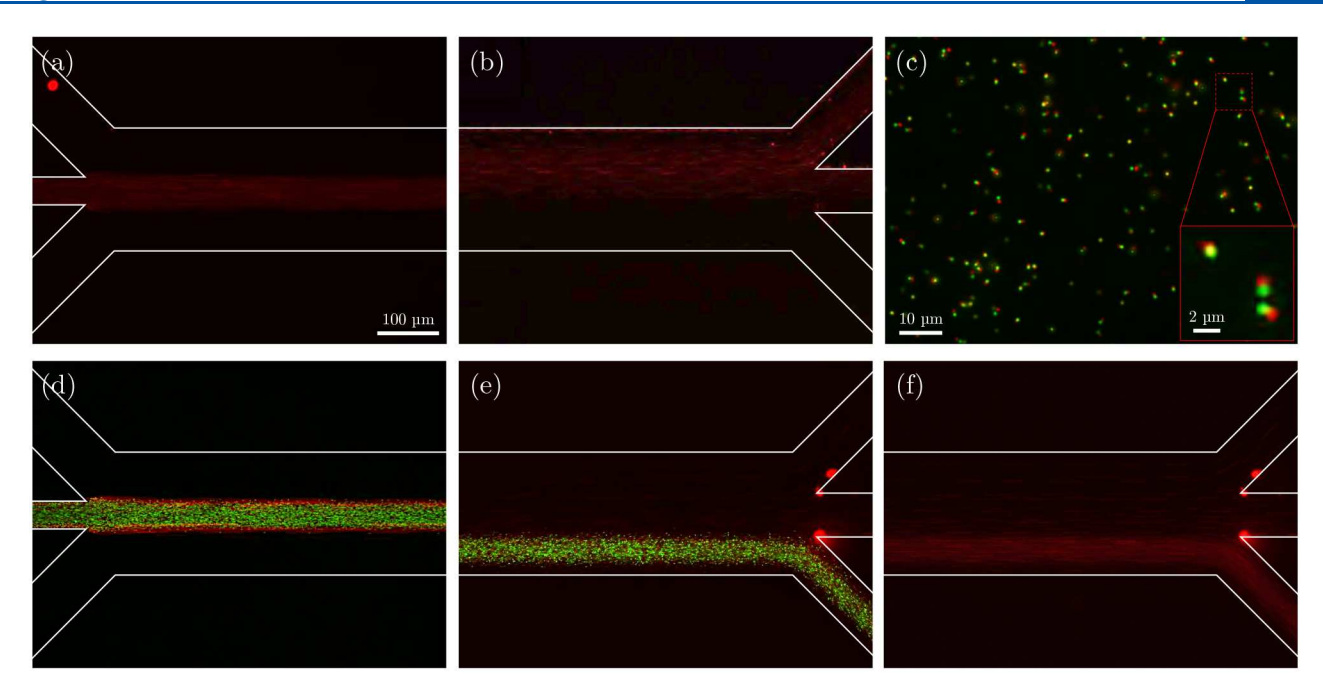


Figure 6. Diffusiophoretic separation of nanoemulsion by the use of diffusiophoresis of vehicle particles. (a, b) Fluorescence images of decane drops near (a) the inlet and (b) the outlet regions. (c) A fluorescence image of cPS-decane mixture. Green indicates cPS and red indicates decane drops. The inset is a close-up image showing aggregation of cPS and decane drops. (d-f) Fluorescence images of cPS-decane mixture near (d) the inlet and (e) the outlet regions. Panel (f) shows the same results as panel (e) but with only decane drops visible.

lower mobility, compared to the larger particles in an NaCl solution of similar ionic strength. Figure 5b presents the experimental dynamics of a mixture of cPS and nanoparticles in our system, demonstrating that both particles significantly deflect toward the positive x-direction (green = cPS, red = nanoparticles). However, because of the small size of the nanoparticles, their enhanced diffusion is also observed through variations in the width of the particle stream over the length of the channel, resulting in a more rapidly decaying distribution (Figure 5c). For a flow-based separation technique that relies on the balance of diffusion and advection effects (e.g., T-sensor⁵⁷), the addition of a size-dependent diffusiophoresis mechanism, such as we achieve here, adds a degree of freedom to precisely control the particle positions and, ultimately, the particle composition of the outlet streams.

Separation of Nanoemulsions Using Carrier Vehicle Particles. Given that highly charged particles can be effectively manipulated using the current system, we also demonstrate that particles with low surface charge can also be separated using more highly charged particles as a "vehicle," provided that the particles of interest can adhere to the charged vehicle particle. As a proof of concept, consider the separation of nanoemulsions, which is typically difficult to achieve. S8,59 As shown in Figures 6a and 6b, a stream of decane nanoemulsion displays only a weak deflection toward the CO₂ side, implying the drops are slightly positively charged.

However, upon mixing the decane nanoemulsion with the cPS particles, the decane droplets wet the cPS particles and form particle—drop pairs, as shown in Figure 6c. This pairing facilitates the separation of the nanoemulsion through the manipulation of the larger, more highly charged particles as vehicles to carry nanodroplets through a degree of separation that would not have been possible in a simple nanoemulsion. We demonstrate this separation enhancement in Figures 6d—f, where a mixture of cPS and decane oil drops is seen to deflect

to a higher degree than the simple case of decane oil drops alone. Indeed, the trajectories of the decane droplets in this case practically overlap with the trajectories of the cPS particles (Figure 6e). For a clear comparison, Figure 6f shows only the decane drops (red) from the same results shown in Figure 6e. Possible applications to exploit this coupling between particle droplet interaction and diffusiophoresis include enhanced oil recovery post-processing technologies. In an oil-water emulsion extracted from a reservoir or a wastewater for instance, emulsified oil drops are relatively insensitive to many separation techniques, such as sedimentation and centrifugal processes.⁶⁰ The introduction of charged particles in these emulsions to induce particle-droplet aggregation and serve as carrier particles, followed by a crossflow separation could thus be utilized to achieve efficient droplet separations for even a weakly charged or noncharged emulsion.

CONCLUSION

To summarize, we have demonstrated a crossflow colloid separation enabled by CO₂-induced diffusiophoresis. Because of the excellent permeability of PDMS, a simple, monolithic channel design was utilized for the colloid separation. The solutes produced by the dissolution of CO₂ gas enabled strong electrolytic diffusiophoresis, allowing the particle to migrate both down and up the solute gradients, depending on the colloid surface charge. Also, the competition between electrophoresis and chemiphoresis enabled a size-dependent colloid manipulation. We have further shown that nanoemulsions can be effectively separated by the use of charged colloidal particles as carrier vehicles. The proposed particle manipulation that relies on particle—particle interaction can also be used for other biomedical applications, such as the separation of tumor cells⁶¹ or targeted drug delivery.⁶²

AUTHOR INFORMATION

Corresponding Author

*E-mail: sangwoos@hawaii.edu.

ORCID ®

Sangwoo Shin: 0000-0001-5618-8522

Notes

The authors declare no competing financial interest.

ACKNOWLEDGMENTS

This material is based on work supported by the National Science Foundation, under Grant No. CBET-1930691.

REFERENCES

- (1) Akagi, T.; Ichiki, T. Cell electrophoresis on a chip: what can we know from the changes in electrophoretic mobility? *Anal. Bioanal. Chem.* **2008**, *391*, 2433.
- (2) Wang, X. B.; Yang, J.; Huang, Y.; Vykoukal, J.; Becker, F. F.; Gascoyne, P. R. Cell separation by dielectrophoretic field-flow-fractionation. *Anal. Chem.* **2000**, *72*, 832–839.
- (3) Petersson, F.; Aberg, L.; Sward-Nilsson, A. M.; Laurell, T. Free flow acoustophoresis: microfluidic-based mode of particle and cell separation. *Anal. Chem.* **2007**, *79*, 5117–5123.
- (4) Vigolo, D.; Rusconi, R.; Stone, H. A.; Piazza, R. Thermophoresis: microfluidics characterization and separation. *Soft Matter* **2010**, *6*, 3489–3493.
- (5) Di Carlo, D. Inertial microfluidics. Lab Chip 2009, 9, 3038-3046
- (6) MacDonald, M. P.; Spalding, G. C.; Dholakia, K. Microfluidic sorting in an optical lattice. *Nature* **2003**, 426, 421.
- (7) Pamme, N.; Manz, A. On-chip free-flow magnetophoresis: continuous flow separation of magnetic particles and agglomerates. *Anal. Chem.* **2004**, *76*, 7250–7256.
- (8) Abécassis, B.; Cottin-Bizonne, C.; Ybert, C.; Ajdari, A.; Bocquet, L. Boosting migration of large particles by solute contrasts. *Nat. Mater.* **2008**, *7*, 785–789.
- (9) Palacci, J.; Abecassis, B.; Cottin-Bizonne, C.; Ybert, C.; Bocquet, L. Colloidal motility and pattern formation under rectified diffusiophoresis. *Phys. Rev. Lett.* **2010**, *104*, 138302.
- (10) Brady, J. F. Particle motion driven by solute gradients with application to autonomous motion: continuum and colloidal perspectives. *J. Fluid Mech.* **2011**, *667*, 216–259.
- (11) Annunziata, O.; Buzatu, D.; Albright, J. G. Protein diffusiophoresis and salt osmotic diffusion in aqueous solutions. *J. Phys. Chem. B* **2012**, *116*, 12694–12705.
- (12) Yadav, V.; Freedman, J. D.; Grinstaff, M.; Sen, A. Bone-Crack Detection, Targeting, and Repair Using Ion Gradients. *Angew. Chem., Int. Ed.* **2013**, 52, 10997–11001.
- (13) Florea, D.; Musa, S.; Huyghe, J. M.; Wyss, H. M. Long-range repulsion of colloids driven by ion exchange and diffusiophoresis. *Proc. Natl. Acad. Sci. U. S. A.* **2014**, *111*, 6554–6559.
- (14) Kar, A.; Guha, R.; Dani, N.; Velegol, D.; Kumar, M. Particle Deposition on Microporous Membranes Can Be Enhanced or Reduced by Salt Gradients. *Langmuir* **2014**, *30*, 793–799.
- (15) Kar, A.; Chiang, T.-Y.; Ortiz Rivera, I.; Sen, A.; Velegol, D. Enhanced transport into and out of dead-end pores. *ACS Nano* **2015**, *9*, 746–753.
- (16) Paustian, J. S.; Angulo, C. D.; Nery-Azevedo, R.; Shi, N.; Abdel-Fattah, A. I.; Squires, T. M. Direct measurements of colloidal solvophoresis under imposed solvent and solute gradients. *Langmuir* **2015**, *31*, 4402–4410.
- (17) Shin, S.; Um, E.; Sabass, B.; Ault, J. T.; Rahimi, M.; Warren, P. B.; Stone, H. A. Size-dependent control of colloid transport via solute gradients in dead-end channels. *Proc. Natl. Acad. Sci. U. S. A.* **2016**, *113*, 257–261.
- (18) Banerjee, A.; Williams, I.; Azevedo, R. N.; Helgeson, M. E.; Squires, T. M. Solutoinertial phenomena: Designing long-range, long-

lasting, surface-specific interactions in suspensions. *Proc. Natl. Acad. Sci. U. S. A.* **2016**, *113*, 8612–8617.

- (19) Shi, N.; Nery-Azevedo, R.; Abdel-Fattah, A. I.; Squires, T. M. Diffusiophoretic Focusing of Suspended Colloids. *Phys. Rev. Lett.* **2016**, *117*, 258001.
- (20) Stout, R. F.; Khair, A. S. Influence of ion sterics on diffusiophoresis and electrophoresis in concentrated electrolytes. *Phys. Rev. Fluids* **2017**, *2*, No. 014201.
- (21) Shin, S.; Shardt, O.; Warren, P. B.; Stone, H. A. Membraneless water filtration using CO₂. *Nat. Commun.* **2017**, *8*, 15181.
- (22) Shin, S.; Ault, J. T.; Feng, J.; Warren, P. B.; Stone, H. A. Lowcost zeta potentiometry using solute gradients. *Adv. Mater.* **2017**, 29, 1701516.
- (23) Shin, S.; Ault, J. T.; Warren, P. B.; Stone, H. A. Accumulation of Colloidal Particles in Flow Junctions Induced by Fluid Flow and Diffusiophoresis. *Phys. Rev. X* **2017**, *7*, No. 041038.
- (24) Ault, J. T.; Shin, S.; Warren, P. B.; Stone, H. A. Diffusiophoresis in one-dimensional solute gradients. *Soft Matter* **2017**, *13*, 9015–9023
- (25) Moller, F. M.; Kriegel, F.; Kiess, M.; Sojo, V.; Braun, D. Steep pH gradients and directed colloid transport in a microfluidic alkaline hydrothermal pore. *Angew. Chem., Int. Ed.* **2017**, *56*, 2340–2344.
- (26) Nery-Azevedo, R.; Banerjee, A.; Squires, T. M. Diffusiophoresis in Ionic Surfactant Gradients. *Langmuir* **2017**, 33, 9694–9702.
- (27) Friedrich, S. M.; Burke, J. M.; Liu, K. J.; Ivory, C. F.; Wang, T.-H. Molecular rheotaxis directs DNA migration and concentration against a pressure-driven flow. *Nat. Commun.* **2017**, *8*, 1213.
- (28) Shin, S.; Warren, P. B.; Stone, H. A. Cleaning by Surfactant Gradients: Particulate Removal from Porous Materials and the Significance of Rinsing in Laundry Detergency. *Phys. Rev. Appl.* **2018**, 9, No. 034012.
- (29) Ault, J. T.; Shin, S.; Stone, H. A. Diffusiophoresis in narrow channel flows. *J. Fluid Mech.* **2018**, 854, 420–448.
- (30) Yang, F.; Shin, S.; Stone, H. A. Diffusiophoresis of a charged drop. *J. Fluid Mech.* **2018**, 852, 37–59.
- (31) Gupta, A.; Rallabandi, B.; Stone, H. A. Diffusiophoretic and diffusioosmotic velocities for mixtures of valence-asymmetric electrolytes. *Phys. Rev. Fluids* **2019**, *4*, No. 043702.
- (32) Prieve, D. C.; Malone, S. M.; Khair, A. S.; Stout, R. F.; Kanj, M. Y. Diffusiophoresis of charged colloidal particles in the limit of very high salinity. *Proc. Natl. Acad. Sci. U. S. A.* **2019**, *116*, 18257–18262.
- (33) Shin, S.; Doan, V. S.; Feng, J. Osmotic Delivery and Release of Lipid-Encapsulated Molecules via Sequential Solution Exchange. *Phys. Rev. Appl.* **2019**, *12*, No. 024014.
- (34) Banerjee, A.; Squires, T. M. Long-range, selective, on-demand suspension interactions: Combining and triggering soluto-inertial beacons. *Sci. Adv.* **2019**, *5*, eaax1893.
- (35) Warren, P. B.; Shin, S.; Stone, H. A. Diffusiophoresis in ionic surfactants: effect of micelle formation. *Soft Matter* **2019**, *15*, 278–288.
- (36) Battat, S.; Ault, J. T.; Shin, S.; Khodaparast, S.; Stone, H. A. Particle entrainment in dead-end pores by diffusiophoresis. *Soft Matter* **2019**, *15*, 3879–3885.
- (37) Lee, D.; Lee, J. A.; Lee, H.; Kim, S. J. Spontaneous selective preconcentration Leveraged by Ion exchange and Imbibition through nanoporous medium. *Sci. Rep.* **2019**, *9*, 2336.
- (38) Ault, J. T.; Shin, S.; Stone, H. A. Characterization of surface-solute interactions by diffusioosmosis. *Soft Matter* **2019**, *15*, 1582–1596.
- (39) Ha, D.; Seo, S.; Lee, K.; Kim, T. Dynamic Transport Control of Colloidal Particles by Repeatable Active Switching of Solute Gradients. ACS Nano 2019, 13, 12939.
- (40) Chu, H. C.; Garoff, S.; Tilton, R. D.; Khair, A. S. Advective-diffusive spreading of diffusiophoretic colloids under transient solute gradients. *Soft Matter* **2020**, *16*, 238.
- (41) Velegol, D.; Garg, A.; Guha, R.; Kar, A.; Kumar, M. Origins of concentration gradients for diffusiophoresis. *Soft Matter* **2016**, *12*, 4686–4703.

(42) Keh, H. J. Diffusiophoresis of charged particles and diffusioosmosis of electrolyte solutions. *Curr. Opin. Colloid Interface Sci.* **2016**, 24, 13–22.

- (43) Marbach, S.; Bocquet, L. Osmosis, from molecular insights to large-scale applications. *Chem. Soc. Rev.* **2019**, *48*, 3102.
- (44) Anderson, J. L. Colloid transport by interfacial forces. *Annu. Rev. Fluid Mech.* **1989**, 21, 61–99.
- (45) Lee, H.; Kim, J.; Yang, J.; Seo, S. W.; Kim, S. J. Diffusiophoretic exclusion of colloidal particles for continuous water purification. *Lab Chip* **2018**, *18*, 1713–1724.
- (46) Mohajerani, F.; Zhao, X.; Somasundar, A.; Velegol, D.; Sen, A. A theory of enzyme chemotaxis: from experiments to modeling. *Biochemistry* **2018**, *57*, 6256–6263.
- (47) Visan, A.; Lammertink, R. G. Reaction induced diffusio-phoresis of ordinary catalytic particles. *React. Chem. Eng.* **2019**, *4*, 1439–1446.
- (48) Xia, Y.; Whitesides, G. M. Soft lithography. Angew. Chem., Int. Ed. 1998, 37, 550–575.
- (49) Merkel, T. C.; Bondar, V. I.; Nagai, K.; Freeman, B. D.; Pinnau, I. Gas sorption, diffusion, and permeation in poly(dimethylsiloxane). *J. Polym. Sci., Part B: Polym. Phys.* **2000**, 38, 415–434.
- (50) Lee, N. Y.; Chung, B. H. Novel poly(dimethylsiloxane) bonding strategy via room temperature 'chemical gluing. *Langmuir* **2009**, *25*, 3861–3866.
- (51) Palacci, J.; Cottin-Bizonne, C.; Ybert, C.; Bocquet, L. Osmotic traps for colloids and macromolecules based on logarithmic sensing in salt taxis. *Soft Matter* **2012**, *8*, 980–994.
- (52) Staffeld, P. O.; Quinn, J. A. Diffusion-induced banding of colloid particles via diffusiophoresis: 1. Electrolytes. *J. Colloid Interface Sci.* 1989, 130, 69–87.
- (53) Probstein, R. F. Physicochemical Hydrodynamics: An Introduction; John Wiley & Sons, 2005.
- (54) O'Brien, R. W.; White, L. R. Electrophoretic mobility of a spherical colloidal particle. *J. Chem. Soc., Faraday Trans.* 2 **1978**, 74, 1607–1626.
- (55) Prieve, D. C.; Anderson, J. L.; Ebel, J. P.; Lowell, M. E. Motion of a particle generated by chemical gradients. Part 2. Electrolytes. *J. Fluid Mech.* **1984**, *148*, 247–269.
- (56) Keh, H. J.; Wei, Y. K. Diffusiophoretic mobility of spherical particles at low potential and arbitrary double-layer thickness. *Langmuir* **2000**, *16*, 5289–5294.
- (57) Hatch, A.; Kamholz, A. E.; Hawkins, K. R.; Munson, M. S.; Schilling, E. A.; Weigl, B. H.; Yager, P. A rapid diffusion immunoassay in a T-sensor. *Nat. Biotechnol.* **2001**, *19*, 461–465.
- (58) Kota, A. K.; Kwon, G.; Choi, W.; Mabry, J. M.; Tuteja, A. Hygro-responsive membranes for effective oil—water separation. *Nat. Commun.* **2012**, *3*, 1025.
- (59) Solomon, B. R.; Hyder, Md. N.; Varanasi, K. K. Separating oilwater nanoemulsions using flux-enhanced hierarchical membranes. *Sci. Rep.* **2015**, *4*, 5504.
- (60) Zhu, Y.; Wang, D.; Jiang, L.; Jin, J. Recent progress in developing advanced membranes for emulsified oil/water separation. *NPG Asia Mater.* **2014**, *6*, e101.
- (61) Chen, B.; Le, W.; Wang, Y.; Li, Z.; Wang, D.; Lin, L.; Cui, S.; Hu, J. J.; Hu, Y.; Yang, P.; Ewing, R. C.; Shi, D.; Cui, Z. Targeting negative surface charges of cancer cells by multifunctional nanoprobes. *Theranostics* **2016**, *6*, 1887–1898.
- (62) Kagan, D.; Laocharoensuk, R.; Zimmerman, M.; Clawson, C.; Balasubramanian, S.; Kang, D.; Bishop, D.; Sattayasamitsathit, S.; Zhang, L.; Wang, J. Rapid delivery of drug carriers propelled and navigated by catalytic nanoshuttles. *Small* **2010**, *6*, 2741–2747.